Deficits in spatial memory correlate with modified γ-aminobutyric acid type A receptor tyrosine phosphorylation in the hippocampus

Verena Tretter[a,1], Raquel Revilla-Sanchez[b,1], Catriona Houston[a,1], Miho Terunuma[b,1], Robbert Havekes[c,1], Cédrick Florian[c,1], Rachel Jurd[b,1], Mansi Vithlani[a,b], Guido Michels[d], Andrés Couve[e], Werner Sieghart[f], Nicholas Brandon[g], Ted Abel[c], Trevor G. Smart[a], and Stephen J. Moss[a,b,2]

[a]Department of Neuroscience, Physiology and Pharmacology, University College, London WC1E 6BT, United Kingdom; [b]Department of Neuroscience, Tufts University School of Medicine, Boston, MA 02111; [c]Department of Biology, University of Pennsylvania, Philadelphia, PA 19104; [d]Department of Internal Medicine III University of Cologne, 50937 Cologne, Germany; [e]Programa de Fisiología y Biofísica, Universidad de Chile, Independencia 1027, Santiago, Chile; [f]Centre for Brain Research, Medical University of Vienna, Spitalgasse 4, A-1090 Vienna, Austria; and [g]Neuroscience Discovery, Wyeth Research, Princeton, NJ 08852

Edited by Richard L. Huganir, Johns Hopkins University School of Medicine, Baltimore, MD, and approved October 2, 2009 (received for review August 6, 2009)

Fast synaptic inhibition in the brain is largely mediated by γ-aminobutyric acid receptors ($GABA_AR$). While the pharmacological manipulation of $GABA_AR$ function by therapeutic agents, such as benzodiazepines can have profound effects on neuronal excitation and behavior, the endogenous mechanisms neurons use to regulate the efficacy of synaptic inhibition and their impact on behavior remains poorly understood. To address this issue, we created a knock-in mouse in which tyrosine phosphorylation of the $GABA_ARs$ γ2 subunit, a posttranslational modification that is critical for their functional modulation, has been ablated. These animals exhibited enhanced $GABA_AR$ accumulation at postsynaptic inhibitory synaptic specializations on pyramidal neurons within the CA3 subdomain of the hippocampus, primarily due to aberrant trafficking within the endocytic pathway. This enhanced inhibition correlated with a specific deficit in spatial object recognition, a behavioral paradigm dependent upon CA3. Thus, phospho-dependent regulation of $GABA_AR$ function involving just two tyrosine residues in the γ2 subunit provides an input-specific mechanism that not only regulates the efficacy of synaptic inhibition, but has behavioral consequences.

cognition | $GABA_A$ receptor | inhibitory synapses

$GABA_ARs$ are the principal sites of fast synaptic inhibition in the adult brain and are the therapeutic sites of action for benzodiazepines and barbiturates (1, 2). In the adult brain, the majority of benzodiazepine synaptic $GABA_AR$ subtypes are hetero-pentamers that are primarily assembled from α1–3, β1–3, and γ2 subunits (1, 2). A critical determinant for the efficacy of synaptic inhibition is the number of $GABA_ARs$ that are present at inhibitory postsynaptic sites, a process that is subject to dynamic modulation via the phosphorylation of residues within the intracellular domains of individual receptor subunits (3–5, 6, 7). In vitro experiments have revealed that phosphorylation modulates both channel kinetics and receptor membrane trafficking, however the role of $GABA_AR$ phosphorylation in shaping the efficacy of synaptic inhibition and affecting behavior remain unknown (5).

To begin to explore this issue, we have created a knock-in mouse in which the principal sites of tyrosine phosphorylation within $GABA_ARs$, residues Y365 and Y367 within the γ2 subunit, have been mutated to phenylalanines. The resulting animal model provides clear evidence that $GABA_AR$ phosphorylation regulates the efficacy of synaptic inhibition by modulating their membrane trafficking in the endocytic pathway in the brain and also influences some aspects of hippocampal-dependent cognition.

Results

Mutation of Tyrosine Phosphorylation in the γ2 Subunit Results in Embryonic Lethality. To explore the role that phosphorylation of $GABA_ARs$ plays in determining the efficacy of synaptic inhibition, we created a mouse in which the principal sites of tyrosine phosphorylation with the γ2 subunit gene were mutated to phenylalanines (Y365/7F) (Fig. 1*A*). Linearized DNA was used to electroporate mouse 129Sv/PAS derived embryonic stem cells and G418-resistant clones were isolated. DNA was digested with HindIII/BglII, and hybridized with a 3′ probe external to the targeting construct that detected a band of 3.2 kb for untargeted, and 4.2 kb for targeted alleles (Fig. 1*B*). Positive ES-cells were injected into blastocysts, and after confirming germline transmission the resulting heterozygotes were crossed with CMV-Cre mice to delete the *neor* cassette via the cre-loxP system as measured by PCR to amplify a region of intronic sequence surrounding the residual *lox-P* sequence in the targeted allele (Fig. 1*C*). Significantly no neo products were seen in heterozygotes, as measured by PCR. Finally sequencing the respective products demonstrated the presence of the wild-type (YGY) and mutated codons (FGF) in heterozygous mice (Fig. 1*D*). Y365/7F heterozygotes were backcrossed for at least eight generations with C57BL/6J animals. No homozygote pups were born after repeated crossings of the heterozygotes, yielding 67.7% Y365/7F heterozygotes and 32.3% wild-type, consistent with a predicted 2:1 Mendelian ratio for heterozygotes: wild-type ($n > 580$). Empty yolk sacs were observed during some pregnancies at between embryonic stage 10–14 (E10–14), suggesting that homozygotes animals probably die very early on during development.

Reduced Tyrosine Phosphorylation Increased γ2 Expression in the Hippocampus of Y365/7F Heterozygotes. Y365/7 heterozygotes were viable and bred normally, and furthermore, *Nissl* staining of 3-month-old male Y365/7F heterozygote brains did not reveal any gross abnormalities in the structure of the hippocampus (Fig.

Author contributions: V.T., R.R.-S., M.T., R.H., C.F., R.J., M.V., A.C., N.B., T.A., T.G.S., and S.J.M. designed research; V.T., R.R.-S., C.H., M.T., R.H., C.F., R.J., G.M., A.C., N.B., T.A., and S.J.M. performed research; M.V. and W.S. contributed new reagents/analytic tools; V.T., R.R.-S., C.H., M.T., R.H., C.F., R.J., M.V., T.G.S., and S.J.M. analyzed data; and T.A., T.G.S., and S.J.M. wrote the paper.

The authors declare no conflict of interest.

This article is a PNAS Direct Submission.

[1]V.T., R.R.-S., C.H., M.T., R.H., C.F., and R.J. contributed equally to this work.

[2]To whom correspondence should be addressed. E-mail: stephen.moss@tufts.edu.

This article contains supporting information online at www.pnas.org/cgi/content/full/0908840106/DCSupplemental.

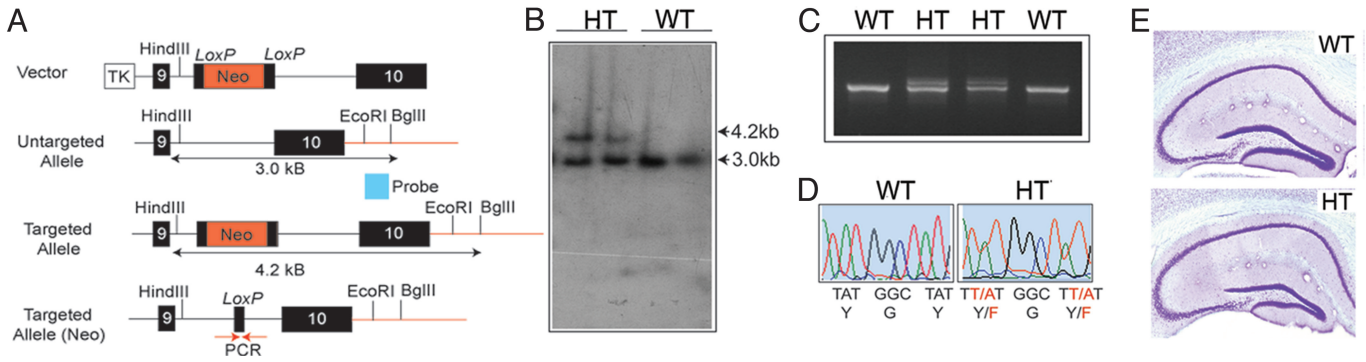

Fig. 1. Generation of Y365/7F knock-in mice. (*A*) Targeting strategy for homologous recombination. Line diagrams representing the targeting construct untargeted and targeted alleles are shown. TK = thymidine kinase, the red lines represent the 3′ flanking genomic DNA, and the red arrows indicate the position of the PCR primers flanking the remaining *loxP* site after *Cre-loxP*-mediated excision of the Neo cassette. The 3′ flanking EcoR1/BglII probe is shown in blue. (*B*) Measuring homologous recombination via Southern blotting. DNA from G418- resistant clones was digested with HindIII/BglII and hydridised with a 3′ probe probe. Two positive clones, as measured by the presence of the additional 4.2-kB band, were then injected into C57BL/6J blastocysts and germ line transmission was confirmed by Southern blotting. (*C*) Y365/7F heterozygotes were crossed with CMV-Cre deletor animals and the excision of the Neo cassette was measured by PCR using the presence of a band of 800-bp representing the target allele and 760-bp the wild-type. (*D*) Genomic DNA spanning exon 10 from wild-type (WT) and Y365/7F heterozygotes (HT) was amplified and sequenced, revealing the presence of the mutated codons. (*E*) Forty-micrometer fixed brain sections from both genotypes were stained with *Nissl* and images were collected by light microscopy (magnification, ×10).

1*E*). To explore the expression levels of the γ2 subunit in the brains of Y365/7F heterozygotes, sections from these and control male mice were stained with anti-γ2 subunit antibodies. As illustrated in Fig. S1, increases in γ2 immunoreactivity were also evident in the cortex of Y365/7F heterozygotes compared to controls.

To further study γ2 subunit expression and phosphorylation in these mutant mice, our studies focused on the hippocampus, because it is a well-defined neuronal circuit with an accepted role in learning and memory formation. Adjacent hippocampal sections from male wild-type and Y365/7F heterozygote mice were stained with a phospho-antibody against Y367 (pY367; Fig. S2) and an anti-γ2 antibody followed by DAB-conjugated secondary antibodies (Fig. 2*A*) to calculate the ratio of pY367: γ2 signals. In wild-type mice, phosphorylation of Y367 was significantly higher in the CA3 region compared to CA1 (Fig. 2*B*; 175.8 ± 5.6% of control; $P < 0.01$), demonstrating subregion specific tyrosine phosphorylation of the γ2 subunit within the hippocampus. In heterozygotes, mutation of Y365/7 significantly decreased Y367 phosphorylation in both CA1 and CA3 regions, to 48.6 ± 4.4 and 62.5 ± 6.9% of control, respectively (Fig. 2*C*) (both $P < 0.01$).

γ2 immunoreactivity in the heterozygotes was significantly increased ($P < 0.01$) to 185 ± 25.2% of control in the CA3 region of the hippocampus, whereas a smaller increase of 134.4 ± 8.9% of control ($P < 0.01$) was evident in CA1 (Fig. 2*D*). To confirm our immunohistochemical experiments, SDS-soluble hippocampal extracts were immunoblotted with pY367 and anti-γ2 antibodies and the ratios of pY367:γ2 were determined. This revealed a significant decrease ($P < 0.001$) in pY367/γ2 ratio in Y365/7F heterozygote animals to 63 ± 11% of wild-type, demonstrating reduced basal phosphorylation of Y367 in Y365/7F mice (Fig. 2*E*).

Thus, mutation of Y365/7 has regional specific effects on γ2 expression levels in the hippocampus, with the largest increases in steady-state accumulation of the γ2 subunit being evident in CA3, which is the region that shows the highest levels of basal Y367 phosphorylation in wild-type animals.

Mutation of Y365/7 Modifies $GABA_AR$ Membrane Trafficking. The effect of mutating Y365/7 on $GABA_AR$ membrane trafficking was measured using biotinylation of hippocampal slices from heterozygous and wild-type mice (8, 9). In hippocampal slices from heterozygotes, the cell surface expression levels of the γ2 subunit were enhanced to 127.6 ± 15.7 of wild-type mice (Fig. 2*F*, $P < 0.05$). In contrast the levels of the NMDA receptor NR2B subunit were unaltered in Y365/7F heterozygotes (Fig. 2*F*).

To explore the mechanism underlying this increased cell surface expression of γ2 subunits in Y365/7F heterozygotes, we focused on possible modifications in endocytosis, as Y365/7 residues have been demonstrated to mediate high affinity binding to the clathrin adaptor AP2, a process disrupted by phosphorylation (5, 10). Incubation of WT and Y365/7F heterozygote slices with myristolated P4 peptide, a characterized cell-permeable inhibitor of $GABA_AR$ endocytosis (11) produced significant increases in the proportion of cell surface γ2 subunits, which was significantly greater for wild-type (249.2 ± 44.6% of control) compared to Y365/7F heterozygote neurons (142.8 ± 8.5% of control; $P < 0.05$) (Fig. 2*G*).

We further examined the effects of mutating Y365/7 on the ability of the γ2 subunit to bind to the clathrin-adaptor AP2 by using synthetic peptides corresponding to amino acids 354–375 in the γ2 subunit. As illustrated in Fig. 2*H*, mutation of Y365/7 drastically reduced the ability of this peptide to bind the μ2 subunit of AP2. Significantly, we have previously documented that mutation of Y365/7 does not compromise $GABA_AR$ functional expression in HEK-293 cells (8). Thus, mutation of Y365/7 leads to enhanced cell surface accumulation of $GABA_ARs$ due to reduced endocytosis and/or modified endocytic sorting.

Size of Inhibitory Synapses Is Increased in the CA3 Region of Y365/7 Heterozygotes. $GABA_AR$ γ2 subunits are highly enriched at inhibitory synapses, where they colocalize with the postsynaptic scaffold protein gephyrin (5, 12–14). Thus we examined whether the increase in total γ2 subunit expression levels seen in Y365/7F heterozygote mice affected the synaptic accumulation of $GABA_ARs$. Focusing on the CA3 region, a significant number of clusters containing both gephyrin and γ2 subunits were observed. These puncta appeared to be enlarged in the heterozygotes (Fig. 3*A*). While the number of γ2/gephyrin puncta per 100 μm^2 was similar between genotypes, there was a significant increase in their size from 7.9 ± 2.5 in wild-type to 13.8 ± 4.3 pixels/puncta in Y365/7F heterozygotes in the CA3 region (Fig. 3*B*; $P < 0.01$). In contrast to CA3, the size and number of γ2/gephyrin puncta were unaltered in CA1 principal neurons from heterozygotes compared to wild-type mice (Fig. 3*B*).

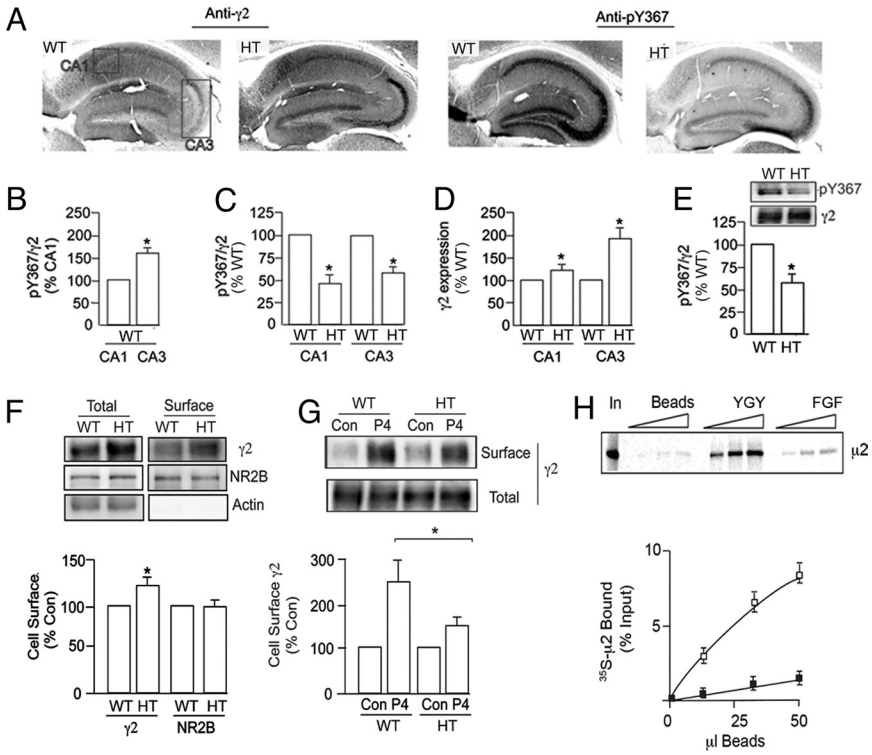

Fig. 2. Analyzing γ2 subunit phosphorylation and expression in the hippocampus of wild-type and Y365/7F heterozygotes. (*A*) Forty-micrometer hippocampal sections section from WT and HT mice were stained with pY367 or anti-γ2 antibodies followed by HRP-conjugated secondaries and DAB staining. The boxes represent the areas of CA1 and CA3 that were used for quantification. (*B*) The mean ratio of pY367/γ2 optical densities in CA1 and CA3 were calculated using stereology and data were normalized to levels in wild-type CA1 (100%). (*C*) The ratio of pY367/γ2 optical densities in CA1 and CA3 regions of the hippocampus of WT and HT mice were calculated and normalized to levels seen in WT (100%). (*D*) γ2 subunit expression levels were quantified by stereolology in CA1 and CA3 regions of WT and HT mice and data were normalized to levels seen in WT (100%). ⋆ indicates significantly different from control ($P < 0.01$) using 40- to 100-μm areas of interest in six individual animals. (*E*) SDS-soluble hippocampal extracts were immunoblotted with anti-pY367 and γ2 antibodies. The ration of pY367/γ2 ratios were then determined and normalized to WT. ⋆ indicates significantly different from control ($P < 0.001$; $n = 3$). (*F*) Cell surface and total fractions from hippocampal slices were immunoblotted with anti-γ2, NR2B, or actin antibodies. The ratio of surface:total γ2 immunoreactivity was determined and normalized to WT (= 100%). (*G*) Hippocampal slices were exposed to 10 μM P4 peptide or vehicle (Con) for 60 min and biotinylated and immunoblotted. Surface: total ratios were then determined and normalized to WT (100%). (*H*) YGY-pep □) or FGF-pep (■) were incubated with ^{35}S-μ2-AP2 and the level of bound ^{35}S was calculated for each peptide. ⋆ = significantly different from control ($P < 0.05$; Student's *t* test, $n = 4$).

mIPSCs Are Selectively Increased in CA3 Hippocampal Neurons from Y365/7 Heterozygotes. Patch clamp recording was used to compare the properties of miniature inhibitory synaptic currents in the respective wild-type and Y365/7F heterozygotes. The mean amplitude of mIPSCs was significantly increased from 25.4 ± 2.3 pA in wild-type to 33.1 ± 2.1 pA ($n = 8$–10; $P < 0.05$) in CA3 neurons from Y365/7F heterozygotes (Fig. 4 *A* and *B*). Examination of the mIPSC amplitude distributions revealed three distinct populations and an increase in the relative proportion of higher amplitude mIPSCs in the heterozygotes (Fig. S3). By comparing the changes between the distributions for wild-type and Y365/7F heterozygote mice, it was apparent that the increase in the mean mIPSC amplitude was caused by an increased frequency of the highest amplitude mIPSCs (Fig. S3). This change was also evident in the cumulative distributions for mIPSC amplitudes, which shifted to higher amplitudes for the heterozygote mice, with the median τ increasing from 18.9 to 26.2 pA (Fig. 4*C*).

The frequency of mIPSCs was also significantly increased from 3.7 ± 0.6 Hz in wild-type to 6.8 ± 0.7 Hz in Y365/7F heterozygotes ($P < 0.05$; $n = 8$–10) (Fig. 4*D*). The distribution of inter-event intervals was again best fit by the sum of three Gaussian populations for the recordings from wild-type and heterozygotes (Fig. S3), with an overall leftward shift in all three Gaussian populations to smaller intervals for events recorded from heterozygotes CA3 neurons. This was also shown by the leftward shift of the cumulative distribution for interevent intervals and the reduction in the median inter-event interval from 188 to 110 ms (Fig. 4*E*). Part of this effect on mIPSC

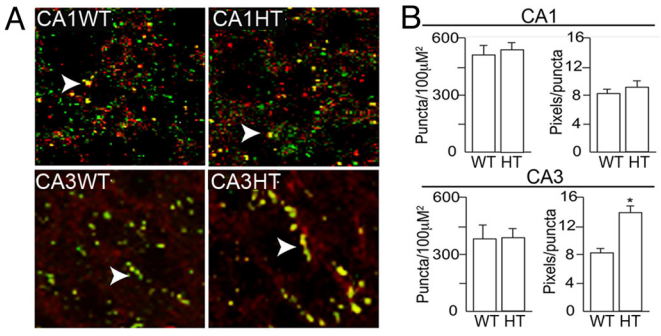

Fig. 3. The size of inhibitory synapses is increased in Y365/7F heterozygotes. (*A*) Forty-micrometer hippocampal slices from WT and HT were stained with antibodies against the γ2 subunit (red) and gephyrin (green) followed by fluorescent secondary antibodies and images were collected from CA1 and CA3 using confocal microscopy. (Scale bar, 20 μm.) (*B*) The number of puncta (defined as an area of fluorescence greater than 1 μm in diameter and at least 2-fold higher fluorescence than background) per 100 μm² were calculated for CA1 and CA3 neurons. The number of pixels per puncta for each genotype was also calculated for 150 puncta per genotype. ⋆ indicates significantly different from control ($P <$ 0.01) using 100–150 areas of interest in six individual animals per genotype.

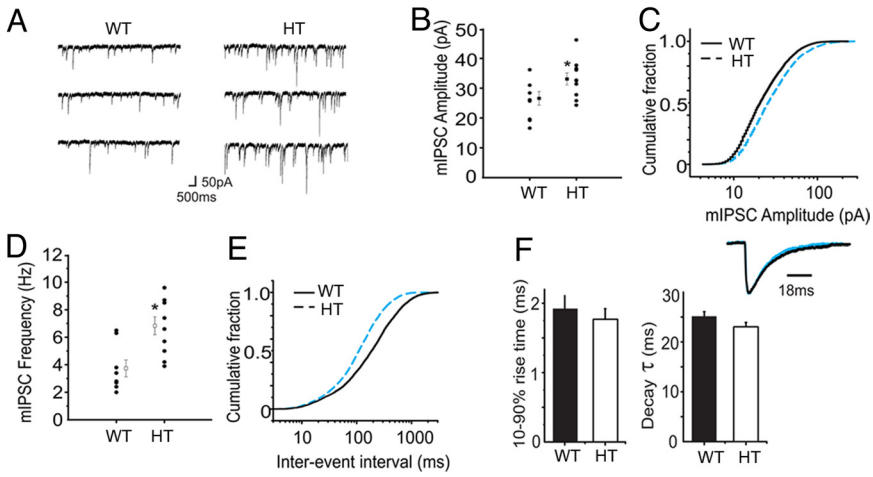

Fig. 4. Synaptic inhibition in CA3 hippocampal pyramidal neurons of Y365/7F heterozygotes. (*A*) Typical recordings of mIPSCs obtained from WT and HT CA3 pyramidal neurons held at −70 mV in the presence of 500 nM TTX, 20 μM CNQX, and 50 μM D-AP5 at 23 °C. (*B*) Mean mIPSC amplitudes (mean ± SEM) are shown for CA3 pyramidal neurons of both genotypes (each data point >400 events). (*C*) Cumulative mIPSC amplitude distributions for WT (black line) and HT (blue, dashed line), $n = 8–10$. (*D*) Mean mIPSC frequencies were calculated from WT and HT CA3 pyramidal neurons (each data point >400 events). (*E*) Cumulative mIPSC inter-event interval distributions for WT (black line) HT (blue, dashed line), $n = 8–10$. (*F*) Ten- to ninety-percent rise-times and single exponential decay times for mIPSCS from WT (black bar) and HT (white bar) CA3 neurons. The inset shows a representative recording of mean scaled (to the peak amplitude) mIPSCs for WT and HT (blue) CA3 neurons.

frequency may reflect our ability to detect an increased number of smaller amplitude events in Y365/7F± animals that previously would have been obscured by the baseline noise (Fig. 4*A*). However, the increased mIPSC amplitude alone is unable to fully account for all of this increase, suggesting that the Y365/7F heterozygous mice also exhibit an increase in presynaptic GABA release.

The kinetics of mIPSCs were also analyzed in the respective genotypes. This revealed very similar kinetics in wild-type (1.9 ± 0.19 ms) and mutant CA3 neurons (1.8 ± 0.15 ms, $n = 8–10$; $P > 0.05$) (Fig. 4*F*). Likewise, the mIPSC decays were best described by single exponentials yielding decay constants (τ) that were indistinguishable between neurons from wild-type (25.2 ± 0.9 ms) and Y365/7F heterozygote (23.2 ± 0.7 ms, $n = 8–10$; $P > 0.05$) animals (Fig. 4*F*). Therefore, in CA3 neurons from Y365/7F+/− mice there was no obvious effect on mIPSC kinetics, but an increase in mean mIPSC amplitude and frequency. This functional effect is consistent with our observation of increased expression levels of $\gamma 2$ subunits in this region, together with their increased accumulation at inhibitory postsynaptic specializations. In addition, this modification of inhibitory synaptic transmission also appears to cause an increase in the level of GABA release.

In contrast, the amplitude, frequency, rise, and decay times of mIPSC in CA1 neurons were unaltered form wild-type and heterozygote mice (Fig. S4). Thus, the efficacy of synaptic inhibition is selectively increased in CA3 compared to CA1 neurons in Y365/7F heterozygote and wild-type mice.

Y365/7F Heterozygotes Exhibit Memory Deficits for Spatial Object Recognition. We next assessed whether the altered levels of inhibition in the CA3 region of Y365/7F heterozygotes had an impact on behavior. First, we determined whether basal locomotor or thigmotaxis activity (an index of exploratory behavior characterized by motion along the walls) was altered in heterozygotes. No differences in these activities were observed between the genotypes when the mice were allowed to explore an open field for 10 min (Fig. S5). Next, we determined whether the mutant mice had altered anxiety-related levels using the zero maze. Wild-type and mutant mice both spent a similar amount of time in the closed arms of the maze, indicating that the mutation in the $GABA_AR$ does not affect anxiety-related behaviors (see Fig. S6). Together these findings indicate that alteration in GABAergic inhibition in CA3 does not alter exploratory and locomotor activity or anxiety–related behaviors.

Next, we assessed whether spatial memory formation was affected in the heterozygotes using the spatial version of the object recognition task. This learning paradigm is based on the ability of animals to discriminate between familiar and novel spatial locations of objects, and performance in this task is critically dependent on hippocampal function, particularly the CA3 region (15, 16). Mice were allowed to explore three distinct objects during the three successive 6 min training sessions and the total exploration time was scored. Mice in both groups gradually decreased the exploration time during consecutive training sessions, suggesting progressive habituation and learning of the spatial configuration of the objects (Fig. 5*A*) [ANOVA, F) (2, 54) = 10.494; $n = 12–17$, $P < 0.001$]. No difference in exploration time was found between the two groups (Fig. 5*A*) [ANOVA, F (1, 27) = 2.021; $P = 0.167$]. On the following day, one of the three objects was placed in a novel spatial location. Wild-type mice preferentially explored the displaced object over the nondisplaced objects, as indicated by a relative increase in exploration time for the displaced object and a decrease in exploration time for the nondisplaced objects (Fig. 5*B*) [paired *t* test t (16) = 2.666 $P < 0.05$]. Strikingly, Y365/7F heterozygotes failed to discriminate between the displaced and nondisplaced objects [Fig. 5*B*, paired *t* test t (11) = −0.412, $P = 0.688$]. These results indicate that enhanced GABAergic inhibition in CA3 impairs memory for spatial configuration.

To determine whether Y365/7F heterozygotes also have a deficit in object recognition memory, 13 wild-type and 18 mutant male mice were subjected to the novel object recognition task. This task uses the differential level of exploration between familiar and unfamiliar (or novel) objects as a behavioral measure for recognition memory and is based on the animal's spontaneous preference for novelty (17). On day 1, mice were allowed to explore the empty arena for 10 min. On the next day, mice received a 10 min training session, during which they were allowed to explore two identical objects placed at symmetric positions from the center of the arena. Both groups spent a similar amount of time on the objects (Fig. 5 *C* and *F*) [(1, 61) =

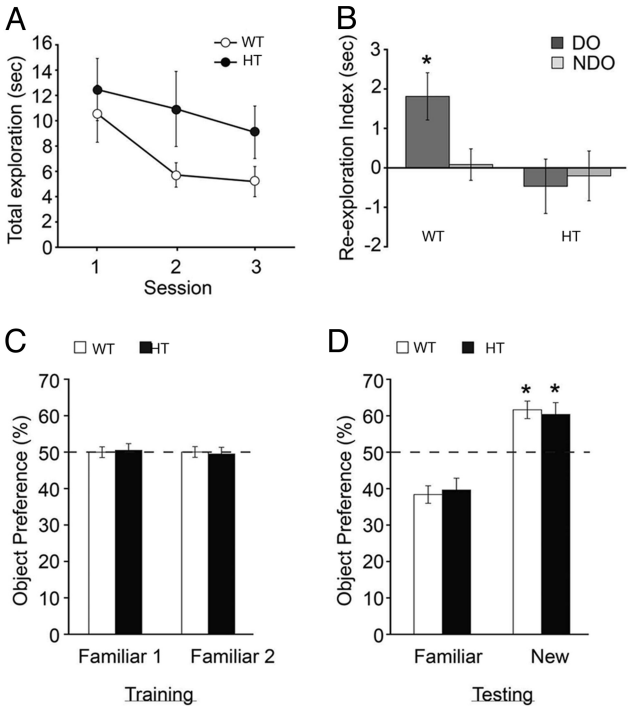

Fig. 5. Y365/7F heterozygote mice are specifically impaired in spatial object recognition. (*A*) The mean time spent exploring two objects was measured for three consecutive 6-min sessions during training. (*B*) The reaction to the displaced object (DO, dark gray histogram) and nondisplaced object (NDO, light gray histogram) was measured 24 h after training. Unlike the WT, HT mice are unable to detect the spatial change in object configuration, ($n = 10$; *, $P < 0.05$). (*C*) The time spent exploring two familiar objects (1 and 2) was measured for 10 min during training for each genotype. (*D*) Preference for one of the original objects (Familiar) and a new object (New) was quantified 24 h after training. Preference for the novel object was expressed as the percentage time spent exploring the novel object relative to the total time spent exploring both objects. The dotted line represents no object preference. *, $P < 0.001$ (compared to familiar object; $n = 13$–18).

0.102; $P = 0.750$]. Twenty-four hours posttraining, mice were reintroduced to the arena and again exposed to two objects, a familiar object and a new object. Both groups preferentially explored the novel object (Fig. 5*D*) [ANOVA, $F(1, 61) = 62.049$; $P < 0.001$]. No genotype or interaction effect between genotype and object was found (Fig. 5*D*) ($P > 0.6$ for both comparisons). This data suggests that facilitated GABAergic signaling in CA3 does not affect memory for objects.

Discussion

Here we have begun to address the significance of phosphorylation in regulating $GABA_AR$ functional expression by creating a knock-in mouse in which the major sites of tyrosine phosphorylation in the γ2 subunit (Y365/7) are mutated to phenylalanines (6,7). Surprisingly, homozygotes for the Y365/7 mutation exhibited a lethal phenotype during embryogenesis. This may suggest a key role for $GABA_ARs$ containing the γ2 subunit during development, assuming that this result does not reflect an unforeseen deficit with the stem cells used to create our knock-in mouse. Consistent with our observation, γ subunit-containing benzodiazepine-sensitive $GABA_ARs$ are important for the development of hindbrain neural networks at E4–5 in the chick (18, 19). Likewise it is emerging that mammalian neuroblast production and their subsequent differentiation is also regulated by benzodiazepine-sensitive $GABA_ARs$ and the γ2 subunit is expressed early during embryonic development in rats and humans (20–22, 23).

In male heterozygotes there were significant increases in the cell surface expression levels of γ2 receptor subunits in the hippocampus, an effect that was mediated by a reduction in their endocytosis and/or endocytic sorting. Thus, Y365/7 residues play a central role in regulating $GABA_AR$ endocytosis in vivo, consistent with their ability to bind AP2 in vitro, an interaction that is negatively regulated by their phosphorylation (5). We noted that in wild-type animals, phosphorylation of pY367 was variable, with the highest levels being evident in CA3. As a consequence of this variation, the Y365/7F mutation had heterogeneous effects on the steady-state accumulation of the γ2 subunit, with the largest increases being evident in CA3 compared with smaller effects in CA1. Thus, these findings suggest that the regulation of $GABA_AR$ γ2 subunit tyrosine phosphorylation could be input specific, which impacts on the steady-state accumulation of these critical inhibitory receptors in distinct hippocampal regions. Consistent with this significant increase in the size, but not the number, of postsynaptic inhibitory specializations was also seen specifically in CA3 (5, 12–14).

We also analyzed mIPSCs in CA1 and CA3 neurons from wild-type and Y365/7F heterozygotes. In CA3 neurons the amplitude and frequency of mIPSCs were increased in heterozygotes. The increase in mIPSC amplitude is in accord with the increased expression levels of the γ2 subunit and the increased size of inhibitory synapses in CA3 pyramidal neurons. The increase in frequency is indicative of altered presynaptic function. In contrast, the properties of mIPSCs were unaltered in CA1 pyramidal neurons from Y365/7F heterozygotes compared to wild-types. Therefore, consistent with the predictions from our imaging studies, inhibitory synaptic transmission is specifically increased in CA3 pyramidal neurons of Y365/7F heterozygotes.

We compared the behavior of these Y365/7F heterozygotes in a hippocampal-dependent and -independent task. We measured whether spatial memory was altered in heterozygotes using a learning paradigm based on the ability of animals to differentiate between familiar and novel spatial locations of objects, a task that is critically dependent upon the CA3 region of the hippocampus (15, 16). Although selectivity for the newly displaced object was evident for wild-type mice, heterozygotes failed to show a preference for the displaced object. In contrast to spatial object recognition, no difference in novel object recognition was seen between genotypes. The regions of the brain that are important for novel object recognition remain controversial, but several fornix lesion studies suggest that the hippocampus is not critical for one-trial object recognition (24).

In summary, our results demonstrate that the mutation of two tyrosine residues in the $GABA_AR$ γ2 subunit profoundly alters phospho-dependent $GABA_AR$ membrane trafficking and receptor number at inhibitory synapses. This critically shapes hippocampal neuronal activity by regulating the cell surface accumulation of $GABA_ARs$ at inhibitory synapses and consequently the efficacy of synaptic inhibition. This leads to dysfunctional hippocampal-dependent learning, highlighting a role for $GABA_AR$ membrane trafficking and its modulation by phosphorylation in determining behavior.

Materials and Methods

Antibodies and Biotinylation. For details see *SI Text*.

Generation of the Y365/7F Knock-In Mouse. An approximately 7.5-kDa SalI/EcoRI genomic sequence encoding the mouse $GABA_AR$ γ2 gene around exons 9 and 10 and flanking introns were subcloned into pBlueScript SK(−). The sequence was then subjected to site-directed mutagenesis to mutate Y365 and Y367 to phenylalanines. The loxP-flanked neomycin (neo) resistance cassette was introduced into the intron downstream of exon 10 and a thymidine kinase expression cassette was inserted downstream of exon 9. The vector was the electroporated into 129Sv/PAS-derived embryonic stem cells and G418- resistant clones were then isolated. Clones were screened via Southern blotting and used to generate chimeric animals, as further documented in the *SI Text*.

Immunohistochemistry. For details see *SI Text*.

Electrophysiology. Slices (350 μm) were perfused in the bath at room temperature with an aCSF containing (mM): 125 NaCl, 2.5 KCl, 1.25 NaH_2PO_4, 26 $NaHCO_3$, 2 $CaCl_2$, 2 $MgCl_2$, and 11 glucose, gassed with 95% O_2/5% CO_2. To block NMDA and AMPA receptor activation, 50 μM AP-5 and 20 μM CNQX were added to the ACSF. Whole-cell voltage-clamp recordings were made from single cells using a MultiClamp 700A amplifier (Molecular Devices) in combination with differential interference contrast microscopy (Nikon eclipse E 600FN), as documented in ref. 12, as further detailed in the *SI Text*.

Behavioral Analysis. For details see *SI Text*.

ACKNOWLEDGMENTS. S.J.M. is supported by National Institute of Neurological Disorders and Stroke Grants NS047478, NS048045, NS051195, NS056359, and NS054900. T.G.S. and S.J.M. are supported by the Medical Research Council and the Wellcome Trust. V.T. was a recipient of a European Union Marie Curie fellowship, M.T. is supported by a fellowship from the American Heart Association, R.H. is supported by a fellowship from the Netherlands Organization for Scientific Research Rubicon Grant 825.07.29 (to R.H.), and R.J. is supported by a National Alliance for Research on Schizophrenia and Depression Young Investigator Award. T.A. and C.F. were supported by National Institute of Mental Health Grant P50MH064045. The support of the Tufts Center for Neuroscience Research, P30 NS047243, is also gratefully acknowledged.

1. Sieghart W, Sperk G (2002) Subunit composition, distribution, and function of $GABA_A$ receptor subtypes. *Curr Top Med Chem* 2:795–816.
2. Rudolph U, Crestani F, Mohler H (2001) $GABA_A$ receptor subtypes: Dissecting their pharmacological functions. *Trends Pharmacol Sci* 22:188–194.
3. Luscher B, Keller CA (2004) Regulation of $GABA_A$ receptor trafficking, channel activity, and functional plasticity of inhibitory synapses. *Pharmacol Ther* 102:195–221.
4. Rudolph U, Mohler H (2006) GABA-based therapeutic approaches: GABAA receptor subtype functions. *Curr Opin Pharmacol* 6:18–23.
5. Jacob TC, Moss SJ, Jurd R (2008) $GABA_A$ receptor trafficking and its role in the dynamic modulation of neuronal inhibition. *Nat Rev Neurosci* 9:331–343.
6. Brandon NJ, Delmas P, Hill J, Smart TG, Moss SJ (2001) Constitutive tyrosine phosphorylation of the $GABA_A$ receptor gamma 2 subunit in rat brain. *Neuropharmacology* 41:745–752.
7. Moss SJ, Gorrie GH, Amato A, Smart TG (1995) Modulation of $GABA_A$ receptors by tyrosine phosphorylation. *Nature* 377:344–348.
8. Terunuma M, et al. (2004) $GABA_A$ receptor phospho-dependent modulation is regulated by phospholipase C-related inactive protein type 1, a novel protein phosphatase 1 anchoring protein. *J Neurosci* 24:7074–7084.
9. Terunuma M, et al. (2008) Deficits in phosphorylation of $GABA_A$ receptors by intimately associated protein kinase C activity underlie compromised synaptic inhibition during status epilepticus. *J Neurosci* 28:376–384.
10. Kittler JT, et al. (2008) Regulation of synaptic inhibition by phospho-dependent binding of the AP2 complex to a YECL motif in the $GABA_A$ receptor gamma2 subunit. *Proc Natl Acad Sci USA* 105:3616–3621.
11. Bogdanov Y, et al. (2006) Synaptic $GABA_A$ receptors are directly recruited from their extrasynaptic counterparts. *EMBO J* 25:4381–4389.
12. Sassoe-Pognetto M, Fritschy JM (2000) Mini-review: Gephyrin, a major postsynaptic protein of GABAergic synapses. *Eur J Neurosci* 12:2205–2210.
13. Sassoe-Pognetto M, et al. (1995) Colocalization of gephyrin and $GABA_A$ -receptor subunits in the rat retina. *J Comp Neurol* 357:1–14.
14. Sassoe-Pognetto M, Panzanelli P, Sieghart W, Fritschy JM (2000) Colocalization of multiple $GABA_A$ receptor subtypes with gephyrin at postsynaptic sites. *J Comp Neurol* 420:481–498.
15. Stupien G, Florian C, Roullet P (2003) Involvement of the hippocampal CA3-region in acquisition and in memory consolidation of spatial but not in object information in mice. *Neurobiol Learn Mem* 80:32–41.
16. Hunsaker MR, Allan KD, Kesner RP (2007) Role of dCA3 efferents via the fimbria in the acquisition of a delay nonmatch to place task. *Hippocampus* 17:494–502.
17. Ennaceur A, Delacour J (1988) A new one-trial test for neurobiological studies of memory in rats. 1: Behavioral data. *Behav Brain Res* 31:47–59.
18. Fortin G, Jungbluth S, Lumsden A, Champagnat J (1999) Segmental specification of GABAergic inhibition during development of hindbrain neural networks. *Nat Neurosci* 2:873–877.
19. Lumsden A, Gulisano M (1997) Neocortical neurons: Where do they come from? *Science* 278:402–403.
20. Laurie DJ, Seeburg PH, Wisden W (1992) The distribution of 13 $GABA_A$ receptor subunit mRNAs in the rat brain. II. Olfactory bulb and cerebellum. *J Neurosci* 12:1063–1076.
21. Liu X, Wang Q, Haydar TF, Bordey A (2005) Nonsynaptic GABA signaling in postnatal subventricular zone controls proliferation of GFAP-expressing progenitors. *Nat Neurosci* 8:1179–1187.
22. Wang DD, Krueger DD, Bordey A (2003) GABA depolarizes neuronal progenitors of the postnatal subventricular zone via $GABA_A$ receptor activation. *J Physiol* 550:785–800.
23. Kanaumi T, Takashima S, Iwasaki H, Mitsudome A, Hirose S (2006) Developmental changes in the expression of $GABA_A$ receptor alpha 1 and gamma 2 subunits in human temporal lobe, hippocampus and basal ganglia: An implication for consideration on age-related epilepsy. *Epilepsy Res* 71:47–53.
24. Bussey TJ, Duck J, Muir JL, Aggleton JP (2000) Distinct patterns of behavioural impairments resulting from fornix transection or neurotoxic lesions of the perirhinal and postrhinal cortices in the rat. *Behav Brain Res* 111:187–202.